UNIVERSITY OF CALIFORNIA,
IRVINE

Multi-wavelength Photomagnetic Imaging for Oral Cancer

THESIS

submitted in partial satisfaction of the requirements
for the degree of

MASTER OF SCIENCE

in Biomedical Engineering

by

Michael Marks

Thesis Committee:
Associate Professor Gultekin Gulsen, chair
Professor Bruce Tromberg
Professor Lydia Su

2017

DEDICATION

To

my wonderful parents, Mike and Maura Marks

in recognition of their unyielding support

TABLE OF CONTENTS

LIST OF FIGURES

LIST OF TABLES

LIST OF EQUATIONS

ACKNOWLEDGMENTS

I would like to express my deepest gratitude to Dr. Gultekin Gulsen for the opportunity to work with his research team at the Center for Functional Onco Imaging. As my advisor, Dr. Gulsen directed my efforts and skills into productive research and fostered the growth that I required to succeed in a high-level research environment. I would also like to thank Dr. Bruce Tromberg for the guidance and mentorship he has provided me since I was an undergraduate.

My lab mates and fellow researchers provided me with unquantifiable help in accelerating my understanding of multimodal imaging.

Finally, I would like to thank all my family and friends for their wholehearted support. Thank you to my parents and my wonderful girlfriend. I would not be who I am without you. Thank you.

ABSTRACT OF THE THESIS

Multi-wavelength Photomagnetic Imaging for Oral Cancer

By

Michael Marks

Master of Science in Biomedical Engineering

University of California, Irvine, 2017

Professor Gultekin Gulsen, Chair

In this study, a multi-wavelength Photomagnetic Imaging (PMI) system is developed and evaluated with experimental studies.. PMI measures temperature increases in samples illuminated by near-infrared light sources using magnetic resonance thermometry. A multiphysics solver combining light and heat transfer models the spatiotemporal distribution of the temperature change. The PMI system develop in this work uses three lasers of varying wavelength (785 nm, 808 nm, 860 nm) to heat the sample. By using multiple wavelengths, we enable the PMI system to quantify the relative concentrations of optical contrast in turbid media and monitor their distribution, at a higher resolution than conventional diffuse optical imaging. The data collected from agarose phantoms with multiple embedded contrast agents designed to simulate the optical properties of oxy- and deoxy-hemoglobin is presented. The reconstructed images demonstrate that multi-wavelength PMI can resolve this complex inclusion structure with high resolution and recover the concentration of each contrast agent with high quantitative accuracy. The modified multi-wavelength PMI system operates under the maximum skin exposure limits defined by the American National Standards Institute, to enable future clinical applications.

Chapter 1

INTRODUCTION

1.1 Oral Cancer

Oral cancer is both highly dangerous and widespread in the United States. The oral cavity is among the ten most common sites affected by cancer worldwide [1]. Human papillomavirus (HPV), recently popularized as a causal factor in cervical cancer, has been implicated in the formation of oral cancer along with cigarette, cigar, pipe smoking, and alcohol consumption [2]. However, oral cancer remains very difficult to diagnose due to lack of developed imaging modalities. In 2012 alone there were over forty thousand identified cases of oral cancer and approximately eight thousand resultant deaths [1]. There are several techniques in development that attempt to use autofluorescence to image and diagnose oral cancer [3].

Figure 1.1 Oral Carcinoma. [4]

Worldwide, 45,000 new cases of oral cancer are anticipated each year while the American Cancer Society estimates 45,780 cases in USA this year, causing 8,650 deaths. Despite easy self-examination and physical examination, patients often present with advanced-stage disease, which is defined by invasion of structures such as deep muscle of the tongue, maxillary sinus, medullary bone, and skin of chin, nose, or face. Generally, the size of these tumors is more than 4cm and they have great propensity for metastasis to the regional lymph nodes in the neck. Since most of these tumors are visible to the naked eye, conventional oral exploration and palpation constitute the first step in the study and diagnosis of oral cancer, the definitive diagnosis being established by histological study of the biopsy specimen. However, correct disease staging requires the use of complementary imaging techniques capable of offering additional information, particularly the depth of invasion of the primary tumor. Depth of invasion not only affects treatment planning but also is a well-established predictor of recurrence and survival. Studies showed that oral tumors in deep tissue layers at the resection margin were associated with increased recurrence rates. Thus, securing sufficient margins, particularly deep margins, is important. A tumor mass is not planar, but rather is a three-dimensional structure; consequently, incomplete resection can result when a surgeon considers only the surface area with no knowledge of invasion depth. Therefore, a preoperative accurate assessment of invasion depth is essential for obtaining sufficiently deep cancer free margins. With the recent advent of the transoral robotic or laser surgery for oral cancers, the preoperative assessment of invasion depth is indeed proven to be more important due to the lack of tactile sensation that gives surgeon clues about the invasion depth in conventional surgery.

Conventional histology has been used as the primary tool to study tissue architecture since the early part of the nineteenth century [5].

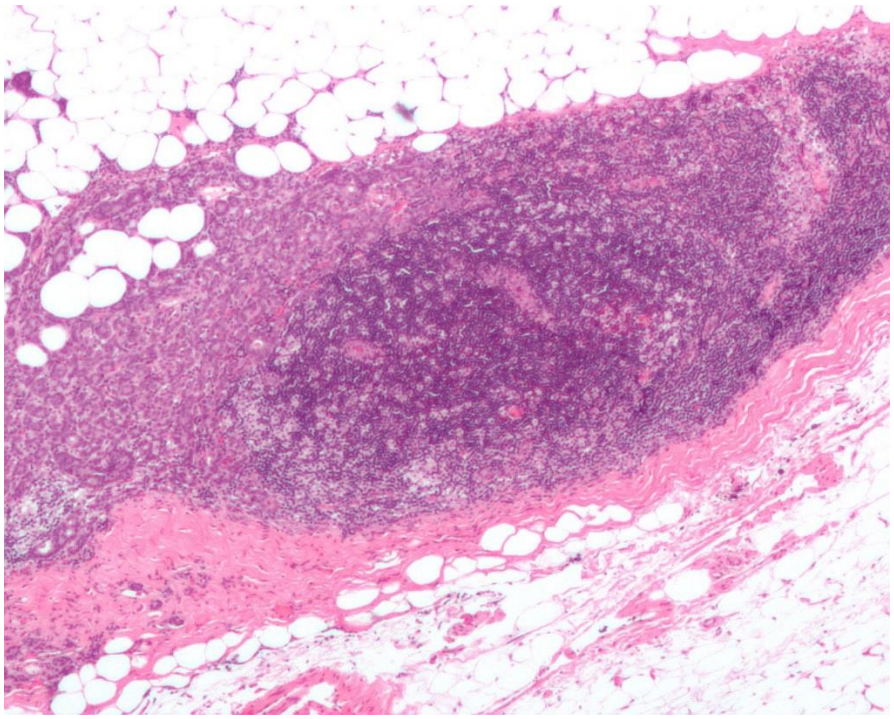

Figure 1.2 Lymph node invaded by breast carcinoma. H&E reveals high concentration of DNA RNA and Ribosomes in the form of dark purple, typical of cancer [6]

Since inception it has been highly valued for its technological simplicity. Using only an appropriate dye and a light microscope tissue can be evaluated. However, histology boasts two often overlooked disadvantages from more modern imaging techniques. First, histology requires a tissue sample, usually collected through biopsy. Because of this, a construction of a histology slide is inherently invasive. Although biopsy is simple in some situations (i.e. in the case of surface cancers) it can be highly complicated in others (i.e. MR-Guided breast cancer biopsy). Other imaging modalities may be of benefit in such high complexity cases. Second, biopsy is in

most cases uncomfortable for patients and in some cases highly invasive. Biopsy is often painful and sometimes requires the use of anesthetic. As with its often-high complexity, the problems associated with its invasiveness can be overcome by using alternate imaging modalities.

1.2 Optical Imaging Technologies for Oral Cancer

Optical imaging techniques offer a non-invasive, cost effective solution to many challenges posed in onco-imaging. Recently, such techniques are beginning to gain traction in clinical research and practice demonstrating their worth and the value of the data which they produce. They are particularly popular because MRI is expensive and x-ray based techniques pose known risks associated with ionizing radiation [7].

1.2.1 Microscopic Techniques

Microscopic techniques produce two dimensional images. First, spatially modulated structured light has been demonstrated to produce quantitative images of absorption contrast. Raman spectroscopy has been used to discriminate normal, inflammatory, premalignant and malignant lesions in the oral cavity through the pronounced differences between their spectral profiles [8]. Also applicable to oral cancer is cutting edge research regarding the use of OCT in conjunction with the Syrian golden hamster model for oral dysplasia [9]. Recent advancement has demonstrated that OCT and optical Doppler tomography can be used to map changes through carcinogenesis in the hamster cheek pouch model with a high sensitivity [10]. These methods are very cost effective but are limited in their resolution compared to MRI based techniques. They

do, however, give clinicians and researchers the ability to quantify the influence of various endogenous and exogenous chromophores.

1.2.2 Structural Techniques

Diffuse optical tomography poses a noninvasive solution to characterizing the optical properties of tissue [11]. Research has circulated over the past ten years detailing its use as a non-ionizing alternative to x-ray mammography. Specifically diffuse optical spectroscopy and imaging (DOSI) is capable of extracting quantify multiple contrast agents [11]. Current efforts are being made to produce standalone DOSI platforms for clinicians to integrate into their practice. Such techniques could conceivably be applied to various other types of cancer including oral.

Further, diffuse optical tomography (DOT) has been studied for its ability to recover functional information from the absorption and scattering of turbid media [12]. However, the high reduced scattering coefficient of tissue greatly hinders the spatial resolution of DOT. In addition to this, DOT measures only at the boundary of samples resulting in a severely ill-posed inverse problem during reconstruction. Diffuse optical tomography is capable of providing density discrimination which can be used to identify cancers in tissue. Unfortunately, the spatial resolution of DOT is limited by tissue scattering [13]. The new technique that we have developed in our lab, Photo-magnetic Imaging (PMI) aims to provide an alternative to DOT which overcomes this weakness.

1.3 Photomagnetic Imaging (PMI)

PMI uses a novel detection scheme to measure optical properties by measuring NIR laser induced heat changes in samples using MR thermometry. It seeks to monitor and reconstruct internal temperature variations produced by differing optical absorption properties of samples. By collecting internal measurement PMI reduces the under-determination of the inverse problem found in DOT [14] PMI uses every voxel of the MRT image as a detector. Penne's bio-heat equations coupled with diffusion model the photo-thermal effect inside the subject and a finite element method (FEM) based forward and inverse solver reconstruct the optical absorption characteristics of the sample. These solvers can reconstruct for any contrast agent, whether exogenous or endogenous.

This system will be used to produce accurate thermal and anatomical maps of cancer lesions, while simultaneously estimating the tissue chromophore composition therein. PMI uses laser light to heat the medium under investigation but employs MRT to obtain temperature map of the tissue with high resolution. These 3D temperature maps are further converted into the optical absorption maps using proper modeling of light propagation and heat transfer in tissue. Since PMI acquires 3D measurements from the whole volume, it provides unprecedented resolution compared to conventional optical imaging modalities.

Producing a quantified map of endogenous chromophore concentrations overlaid with an anatomical MRI image would give clinicians a new tool to evaluate, treat, and cure cancers. These functional maps would also provide researches with a new tool to learn about cancer generally as well as fundamental processes like carcinogenesis and metastasis. The chemical

changes governing these processes are not well understood owing to the difficulty of studying them in-vivo. PMI gives us the ability to open a window we have yet to view cancer through. It also offers the ability to quantify exogenous chromophores like gold nanoparticles.

Cutting edge research has demonstrated the ability to produce anti EGFR- conjugated gold nanoparticles to target and diagnose oral cancer [15]. This emergent technology possesses an inherent synergy with the PMI technique. For instance, currently the imaging modality used to track the gold nanoparticles is Surface Plasmon Resonance (SPR). SPR produces high magnification images but fails to acquire deep penetrating anatomical data. Contrary to this, PMI produces higher resolution anatomical images and has better probing depth [15]. This means that such gold nanoparticles would not be limited to surface based imaging techniques. This would enable further research into the applicability of gold nanoparticles to diagnose other types of cancer. Therefore, my focus during research will be to modify the PMI system to use multiple wavelengths of light and in doing so give researchers and clinicians functional molecular info in the form of tissue intrinsic chromophores or exogenous contrast agents. Specifically, I will design the system to be used with the endogenous chromophores oxy- and deoy- hemoglobin as well as exogenous contrast agents, specifically, gold nanoparticles.

These outlined prognostic difficulties are generalizable to many forms of cancer. Any invasive disease will be difficult for clinicians to image, and any more information that can be acquired (i.e. tissue composition or size) will further enable clinicians to understand, diagnose, and cure these dreaded diseases.

1.5 Desired Outcomes

The novel PMI system will allow noninvasive quantified characterization of various tumors. It will provide geometrical information without need for invasive action required by conventional histology, which has not been previously possible owing to limitations in imaging systems. It will also provide a quantitative map of the tissue chromophore useful in diagnosing and furthering the understanding of any type of lesion be it benign or malignant. The research brings together optics and MRI technology to produce a dual mode imaging system which can aid in the study of carcinogenesis. Thus, knowledge gathered from the fields of optics, imaging, and cell biology come together produce a potentially impactful device. The device also has the potential to collect impactful data for any number of tissue studies. Also, the system's ability to characterize exogenous chromophores makes it a great candidate to be used with experimental markers such as the gold nano-particles being developed on campus for cancer detection. The specific impact of multi-wavelength PMI on oncology could, with further transnational study, impact patient comfort and quality of life by providing a noninvasive imaging technique for all forms of cancer. Furthermore, this research could be expanded to utilize other contrast agents to gather similar information from cancers affecting any part of the body. The device could also be used in future studies that would evaluate the possibility of depth of invasion and chromophore distribution as a prognostic factor for staging of squamous cell carcinoma.

1.6 Outline of the Thesis

My aim is to modify an existing single wavelength PMI prototype for use with multiple wavelengths of light. This modification will involve many aspects of engineering design, who's process flow is further outlined in the chapters to come. Details guarding design choices and efforts required to reach the final prototype will be apparent. Furthermore, by modifying the system to use multiple wavelengths, I will enable PMI to provide the same functional information as conventional diffuse optical imaging modalities with higher resolution and quantitative accuracy due to utilization of MRI. Of particular interest is the ability to quantify the contribution of water, fat, oxy- and de-oxy hemoglobin maps as well as exogenous contrast agents to the absorption of a subject. In doing so, PMI will be a low-cost addition to any clinical MRI systems that would enable the further study of how tissue composition relates to the health of a subject. This will be particularly useful in understanding the chemical predictors of tumor growth and metastasis.

1.7 Specific Aims of Research

Specific Aim 1: *Design and build a multi-wavelength PMI device for cancer imaging.*

To overcome the need for conventional histological assessment of invasive disease, I will construct a novel device. This device will be capable of multi-wavelength photo-magnetic imaging of the oral cavity. Such a device has never been available prior. I will make use of; elements gathered from the single wavelength breast cancer and small animal imaging device [13], and conventional design principles as well as my previous three years' experience in optical device design. The main body of the device will be multiple exterior light sources, routed through fiber optic cables so as not to interfere with surrounding MRI. This device will be powered by laser diodes in an adjacent room to avoid potential hazard to patients and clinicians. This follows the original design [13]. In an attempt to optimize the PMI process I plan to use wavelengths that are capable of distinguishing oxy- and deoxy- hemoglobin. Thus, I will require multiple laser diodes. This will allow for better differentiation and characterization of potential tumors in tissue. Development will also require adaptation of the [13] PMI reconstruction algorithm.

Expected Outcomes:

Successful completion of **aim 1** will provide an oral PMI device that enables noninvasive imaging of invasive disease as well as quantification of the contribution of between one and three chromophores.

Specific Aim 2: *Evaluation of System*

To validate the device and reconstruction algorithms phantoms made in the lab will be imaged. The phantom will be a hollow cylinder made in accordance with previous design. It will have two inclusions of differing dyes selected to mimic oxygenated and deoxygenated hemoglobin. The system will be considered to be validated if it can measure the size of the inclusion and successfully quantify the concentration of dye in each inclusion. The system will also need to approximate the absorption coefficient of each dye without the use of *a priori* data.

Expected Outcomes:

Aim 2 will test the capabilities of the novel PMI device produced in **aim 1** using phantoms. A positive correlation between measurements from the PMI image and the known location, concentration, and absorption of each inclusion would demonstrate the viability of noninvasive measurement and characterization of cancers.

Chapter 2

MULTI-WAVELENGTH PMI

2.1 Single-wavelength PMI

Photo-magnetic imaging (PMI) is a multimodal imaging technique that brings together optical imaging and MRI. It produces images with the contrast of diffuse optical tomography and the resolution of magnetic resonance imaging (MRI) [13] by using MR thermometry to measure laser induced temperature changes in a given subject. Currently, PMI uses a single wavelength laser source to heat a tissue sample and uses MR thermometry to provide a high resolution three-dimensional absorption map of the tissue. This chapter will document the instrumentation of a multi-wavelength PMI system and future chapters explore the overarching hypothesis that this novel photo-magnetic imaging device can noninvasively map and quantify the concentration of multiple absorbing agents of a lesion. To test this hypothesis, I will use my knowledge of and bring together the fields of optical physics and magnetic resonance imaging.

Previous papers [13] have documented our lab's development of Photomagnetic Imaging. This included a substantial portion of Dr. Alex Luk's dissertation work. Both of whom lent guidance and help on the modification described in this thesis. Upon my joining the research team the system had a single wavelength illumination source driven and cooled by an off the shelf system. Specifically, they were driven by an ATI ATEI-288-6AE. This was coupled with manufacturer supplied computer controllers. This system was responsible for the pioneering studies published over the last three years.

These papers have established the potential for PMI as a viable imaging technique for various small animal research models. However, they have only produced thermal maps using a single wavelength of light. As stated before, by using multiple wavelengths, the system will be able to produce quantified data about tissue chromophores.

2.2 Multi-wavelength PMI

I will produce a PMI system which uses multi-wavelength illumination. By using multiple wavelengths, the system will be able to provide tissue information beyond that of a heat map. Such capabilities will introduce a multi-physics problem, as both heat and light absorption can be measured. However, through these two measurements both an absorption map and an estimation of tissue chromophores can be acquired. This will more accurately characterize the sample than the current PMI method. The device will be able to quantify both exogenous and endogenous chromophores. Of specific interest is the content of oxy- and deoxy- hemoglobin. In addition to this, I will lower the power output of the illumination source.

2.3 Instrumentation

PMI instrumentation has three major components

1. Laser Diodes
2. Optical Fibers
3. Optical Interface

The substantial majority of my contribution to this project was prototype design and modification. The flow of modification and design process can be easily visualized by a flowchart.

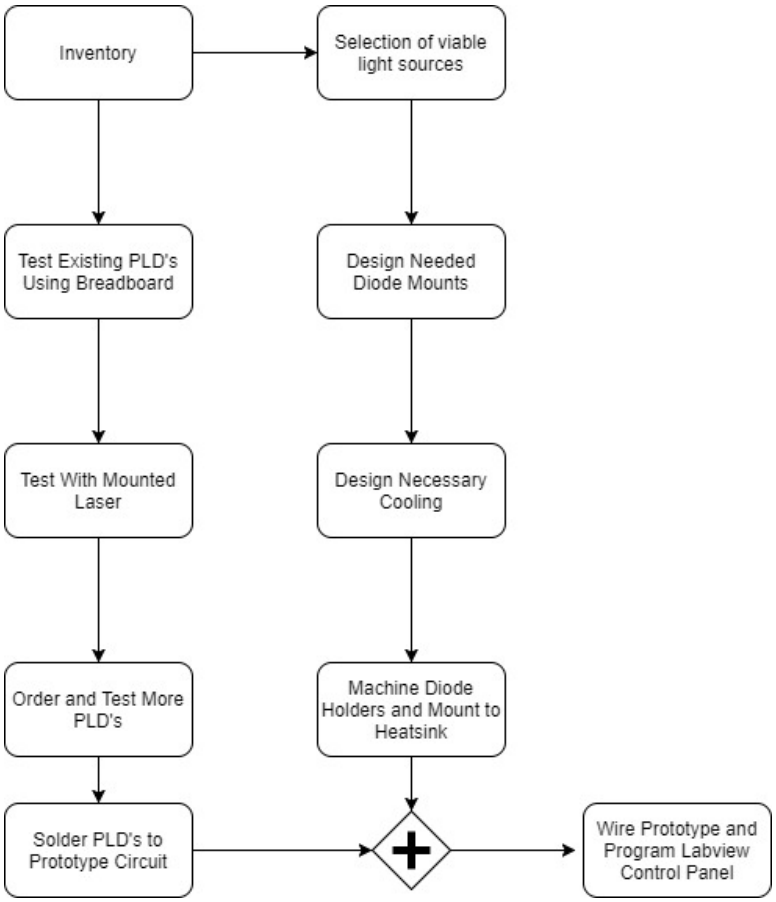

Figure 2.1 Flowchart detailing component selection, design, and fabrication from inventory to final prototype

Key to the modification of the single wavelength system was the addition of three other illumination sources. These sources came in the form of laser diodes and enable us to capture functional data about tissue chromophores. Aside from the addition of these sources, the optical system would need to be computer controlled. For this purpose, LabView is used to build a control panel that interfaced with all necessary components.

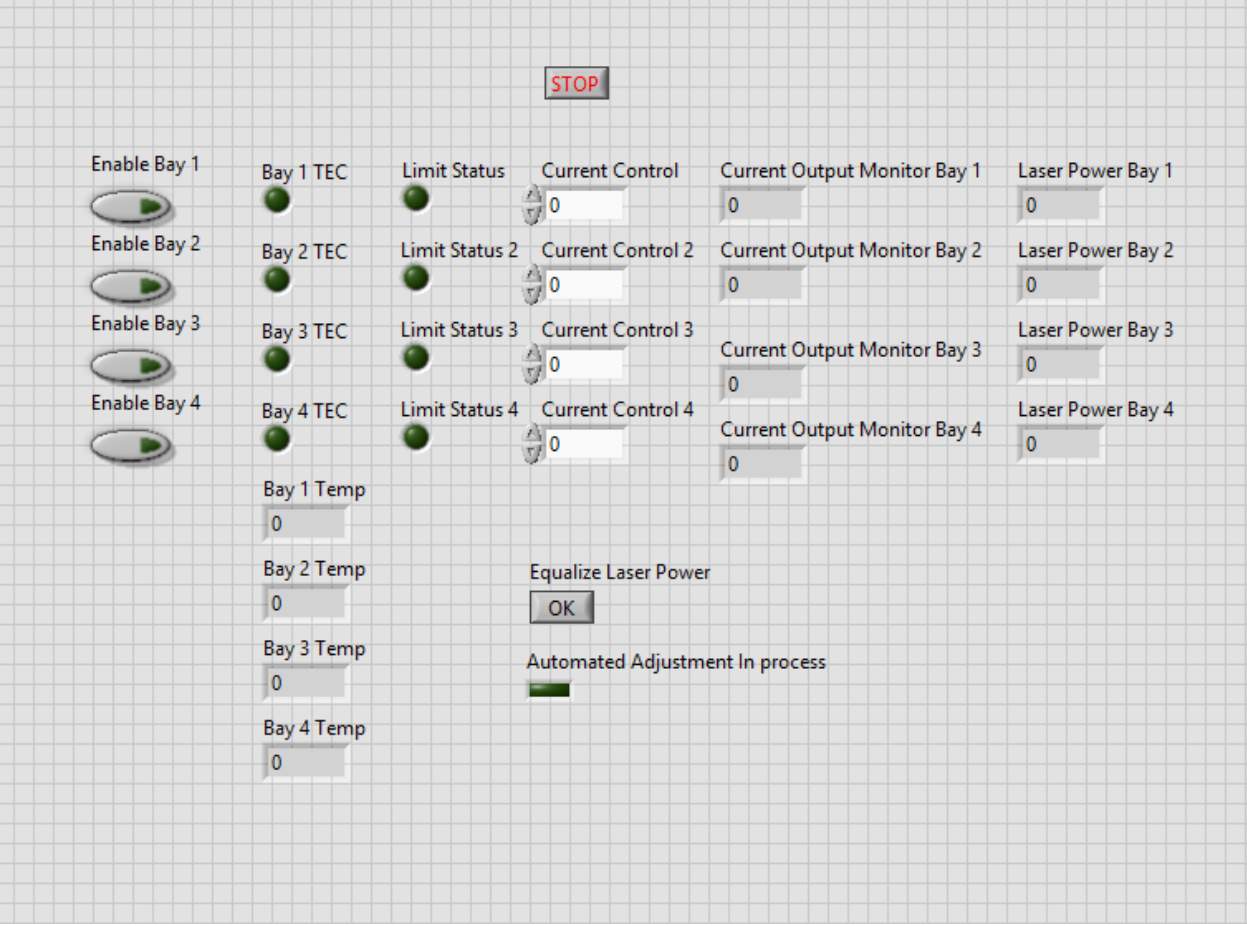

Figure 2.2 LabView PMI control panel

Our system is the first of its kind; its novel construction was completed in house using a combination of purchased and fabricated components. The MRT measurements were performed using a Philips 3 Tesla Achieva system. PRF images were acquired using a gradient echo

sequence using 60 and 12 ms as repetition and ET, respectively. The phantom was mounted in a specially designed small animal MRI coil inside the MR bore. The phantom was illumined using a 785, 808, and 850 nm laser diodes (wslb-780-003-H, FL-FCSE01-7-808-3-200-.22, LDX-3640-860-9-SMA). Laser diodes were selected based on availability and relationship to the isosbestic point of oxy- and deoxy- hemoglobin. By surrounding the isobestic point of oxy- and deoxy- hemoglobin, our system increases its ability to differentiate these two, critical, endogenous chromophores.

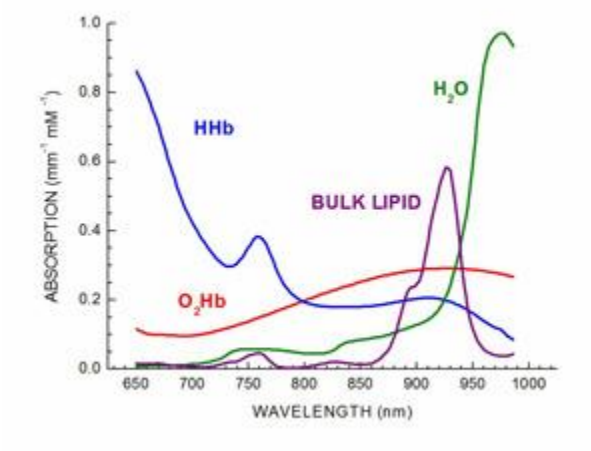

Figure 2.3 Absorption curves of major endogenous chromophores [16]

Lasers are driven by Wavelength Electronics PLD 5000's controlled by National Instruments Labview through a NI6008 USB interface and a CD4081BE logic gate. A Topward 6303D-10 dual tracking power supply provided necessary power to our system. Laser diodes were mounted in copper plates machined in house and cooled by ATEI-288-6AS thermo electric coolers controlled by a VUE Metrix TEC control module. Light was transported to the OMI interface inside the MR bore using a 15m long optical fiber. The interface consists of a RF coil manufactured in house with windows for illumination and ports that can hold the collimation

optics, specifically a 35mm aspherical lens from Newport Optics. Laser power was calibrated according to ANSI limits (.032 W/cm^2 for 808nm) prior to data collection.

2.3.1 Laser Diodes

The selected laser diodes were fairly dissimilar as they were sourced from different companies. Two of the lasers (785 and 808 nm) were pigtailed to an optical fiber, the other required an SMA connector. Their obvious shape differences also made thermal mount to the cooling system differently. The 785 and the 808nm diode mounted flat onto a copper plate while the 860nm diode needed to be mounted through a piece of copper to properly cool. Visible in Table 2.1 all had different power requirements. Their light output powers needed to be set using a power meter by adjusting each lasers supply current before imaging. Despite their differences, after careful balancing power and consideration of each lasers requirement, all were highly effective. All lasers were routed through matching fibers during imaging.

Table 2.1 Laser diode details [17] [18] [19]

	wslb-785-003-H 	FL-FCSE01-7-808-3-200-22 	LDX-3640-860-9-SMA 
Center Wavelength	785nm	808nm	860nm
Output Power	3000mW	2000mW	4620mW
Mode	Multimode	Multimode	Multimode
Package	Enclosed	2 Pin FC	2 Pin FC
Manufacturer	WSLB	Focuslight	LDX
Type	Single Emitter	Single Emitter	Single Emitter
Fiber Type	225uM	125um MM	400um MM
Output	Fiber Coupled	Fiber Coupled	Fiber Coupled
Package Cooling	TEC	Conductive	Conductive
Duty	CW	CW	CW

2.3.2 Laser Diode Drivers

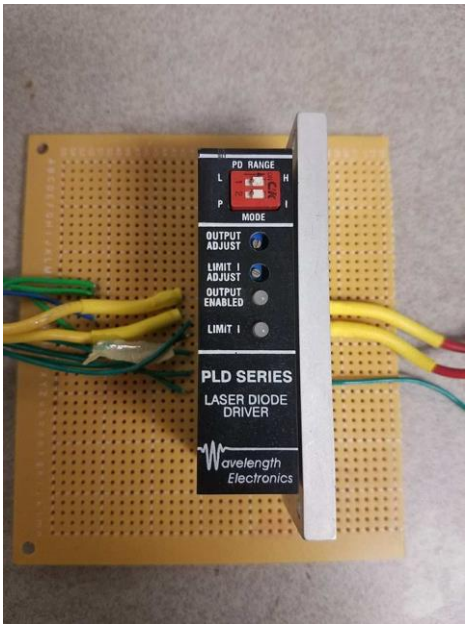

Figure 2.4 PLD5000 on prototype board

Laser Diode Drivers form the backbone of the system. They serve to provide the laser diodes with even, constant current power, ensuring safe and consistent operation. These drivers protect the laser diodes from potentially damaging fluctuations in current. The previous system had not used them as it used an off the shelf diode/TEC driver with a manufacturer included user interface. The new laser diode drivers were Wavelength Electronics PLD5000. As they were previously unused, they had to be tested and their operation needed to be understood before attaching them to the diodes. To do so, I assembled a basic breadboard test circuit according to manufacturer specifications.

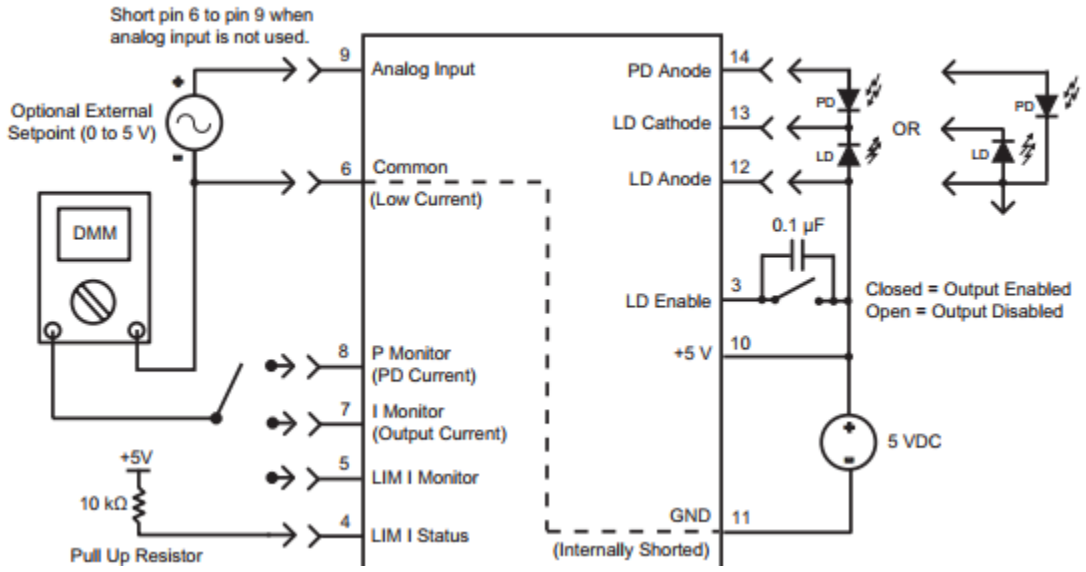

Figure 2.5 Manufacturer specified quick test circuit [20]

A test load consisting of diodes in series simulated the presence of a laser diode on the output and allowed me to test and tune the output current of the laser diode drivers.

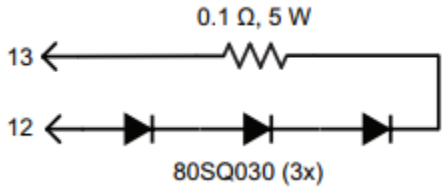

Figure 2.6 PLD test load circuit [20]

Upon testing all twelve PLD5000's , they were ready to be connected to the lasers. However, before powering the lasers up, they had to have a proper cooling system.

2.3.3 Laser Diode Temperature Control System

After selection of laser sources, a thorough study of the necessary techniques for keeping the lasers cool enough to run efficiently became necessary. First, it is necessary to select an appropriate heat sink to cool the lasers. To minimize cost and maximize off the shelf availability, I chose to use a parallel plate-fin heat sink. Using an online tool [21] and the governing equation

$$T_J = P(R_{case} + R_1 + R_2) + T_a \qquad (2.2)$$

to calculate the necessary thermal resistance of the heatsink. During these calculations, I sought to build a system capable of cooling all twelve lasers passively for up to one-minute run time. This would be enough given that we will be using thermo-electric coolers (TEC) for active heat transfer. This added protection would enable the lasers to run indefinitely in the case that future

studies would require longer exposure times and therefore, longer use of the lasers. Finally, the heatsinks were sourced from Heatsink USA because they are extremely reputable and sold a perfect aluminum heatsink at a reasonable price per foot. Below is a cross sectional image of the heatsink selected. Multiple sections will be required to mount all lasers planned for future research.

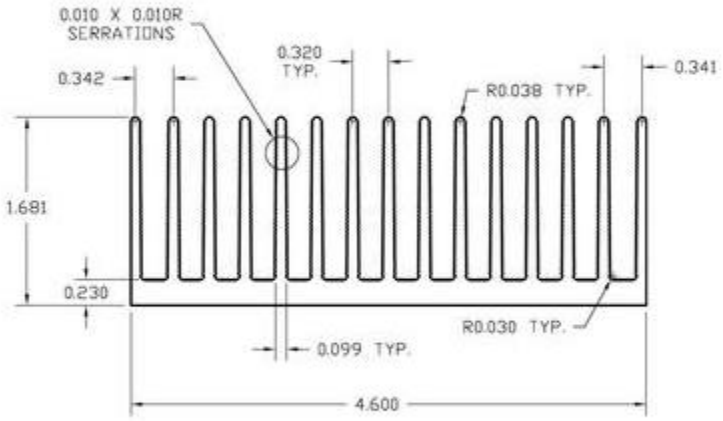

Figure 2.7 Schematic of 4.600: Wide Extruded Aluminum Heatsink. Figure taken from HeatsinkUSA [22]

With the heatsink the heat dissipation problem solved, our lasers will need to be mounted to a copper plate so that heat could be transferred via TEC to the heatsink. This was accomplished entirely in house. A lathe was used to create a copper mount which surrounded the free diodes. I then milled a copper plate and attached all lasers. This plate was mounted to a heatsink with thermal compound and the TEC's in the middle. This provided plenty of cooling power for the lasers and the modular ability to add more lasers as the project progressed.

2.3.4 Optical Interface

Light is transferred from the laser module to the MRI control room through optical fibers approximately 15 meters long. A custom fabricated MRI coil with apertures for laser illumination surrounds the subject. Laser fibers are connected to aspherical collimator lens to produce a more homogenous heat distribution.

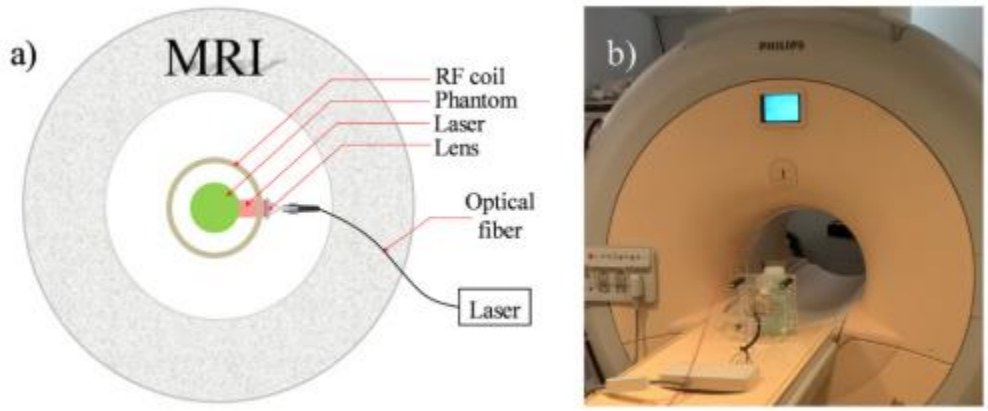

Figure 2.8 a. Schematic of the PMI setup showing the optical instrumentation inside the MRI bore **b**. Picture of optical interface in MRI bore [23]

For prototype purposes, all three fibers were coupled into one lens in the coil. Though imperfect this enabled quick system validation with little induced error owing to the coils large input lens. To produce a better end product with more illumination sources future work will include the addition of an optical multiplexer

2.3.5 Optical Fiber Multiplexing

Although not present in the current prototype, the next necessary component will be an optical multiplexer. This device will enable switching between bays of illumination sources without the use of many fibers or the manual changing of fibers between sources. The multiplexer will work by rotating twelve input fibers in front of four output fibers. As the multiplexer rotates different sets of input and output fibers will be coupled enabling rapid, automated switching of the lasers without disturbing alignment.

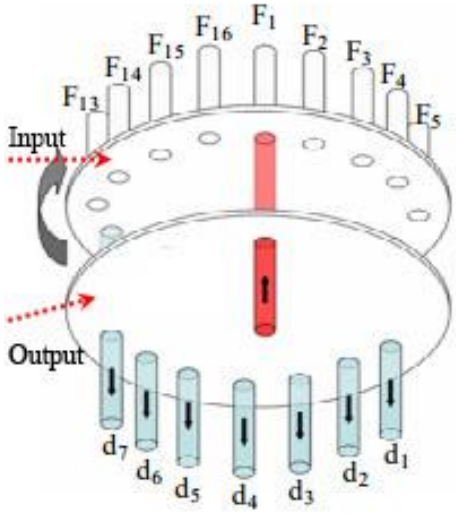

Figure 2.9 Optical Fiber Multiplexer [24]

2.4 Mathematical Modeling

PMI irradiates the tissue with a near-infrared light and monitors the induced temperature increase using MRT. A numerical solver combining light and heat equations is used to model the spatiotemporal distribution of temperature increase. First, it is widely established that the diffusion equation is a useful tool to model the light transport within turbid media [25-27].

$$-\nabla D^{\lambda}(r)\nabla\Phi^{\lambda}(r)+\mu_a^{\lambda}(r)\Phi^{\lambda}(r)=S^{\lambda}(r) \tag{2.2}$$

where $\Phi(r)$ is the photon density at position *r*, μ_a is the absorption coefficient and *D* the diffusion coefficient, $D(r)=1/3(\mu_a+\mu_s^{'})$ with $\mu_s^{'}$ being the reduced scattering coefficient. *S*® is the isotropic source of light. The subscript λ denotes the wavelength of the used light source.

The conversion of photons energy to a thermal energy could be defined as the product of the optical absorption μ_a of the medium and the photon density $\Phi(r)$ at any point of the medium [28, 29]. The Penne's bio-heat thermal equation has been largely used to model the propagation and dynamics of the temperature [30]:

$$\rho c\frac{\partial T^{\lambda}(r,t)}{\partial t}-\nabla k\nabla T^{\lambda}(r,t)=\Phi^{\lambda}(r)\mu_a^{\lambda}(r) \tag{2.3}$$

where ρ is the density, *c* is the specific heat and *k* the thermal conductivity of the medium.

Equation 3.1 and 3.2 are solved using the Neumann boundary conditions and the heat convection boundary condition, respectively [30].

The PMI image reconstruction process is performed iteratively by minimizing the error between the measured $T^m(\lambda)$ and the simulated $T^\lambda\left(\mu_a^\lambda\right)$ temperatures using the following objective function:

$$\Omega\left(\mu_a^\lambda\right)=\sum_{n=1}^{N}\left\|T_n^m(\lambda)-T_n^\lambda(\mu_a^\lambda)\right\|^2 \tag{2.4}$$

where *N* are the number of nodes. The MRT temperature maps $T^m(\lambda)$ are proportional to the phase variations induced by the change in magnetic resonance frequency which is induced by the laser heating. The temperature variation ΔT is described by:

$$\Delta T=\frac{\Delta\phi}{\Gamma} \tag{2.5}$$

where $\Delta\phi=\Delta\phi(t)-\phi(t_0)$ is the difference between the measured MR signal phase, $\phi(t)$, at every pixel at time *t* and the baseline, $\phi(t_0)$, MR signal phase measured at t_0. The constant Γ characterizes the imaging system parameters [31].

2.4.1 Reconstruction of Chromophore Maps

The total absorption of tissue μ_t is equal to the sum of the absorption of all chromophores therein. Generally, this is said to be the combination of; water, oxyhemoglobin, deoxyhemoglobin, and fat. For the purposes of this thesis it can be assumed that fat is not a contributing factor. Thereby we receive;

$$\mu_t = \mu_{water} + \mu_{oxyH} + \mu_{deoxyH} \tag{2.6}$$

It is also known that absorption μ, is equal to concentration (**C**) multiplied by extinction coefficient ε. Thereby we receive with substitution:

$$\mu_t = \varepsilon_{water}\mathbf{C}_{water} + \varepsilon_{oxyH}\mathbf{C}_{oxyH} + \varepsilon_{deoxyH}\boldsymbol{C}_{deoxyH} \tag{2.7}$$

By using three wavelengths of light for multi-wavelength PMI, we can produce three equations for μ_t. With these three equations and known extinction coefficients ε, we have a fully determined system and can solve for concentration of the three major endogenous chromophores.

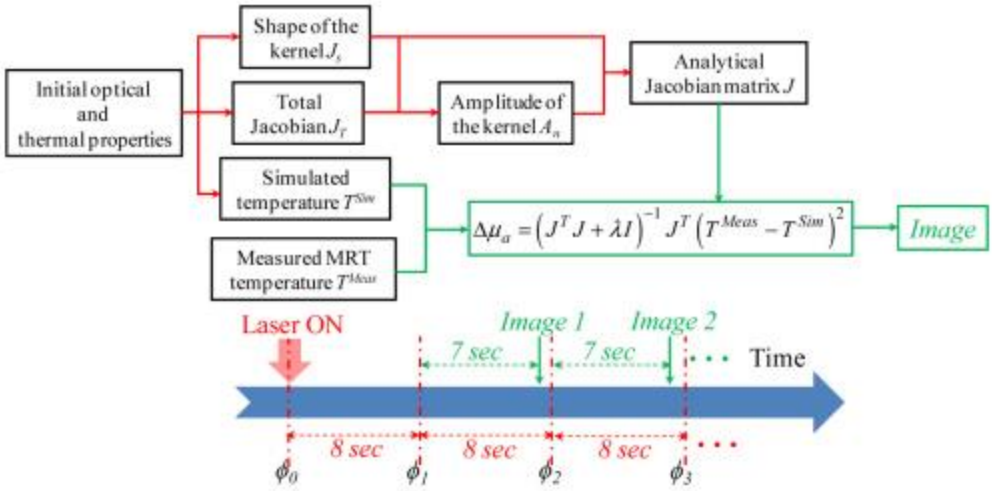

Figure 2.10 Visual representation of PMI image reconstruction [23]

There are two methods that can be used to produce a chromophore map. The first method, solves all of the above equations for each illumination wavelength separately. In doing so it produces a map of the μ_a values of the tissue. These μ_a values can then be converted using known absorption curves to concentration maps for a given set of chromophores. The second method skips calculating absorption completely, thus it is accurately dubbed, direct chromophore reconstruction. Direct chromophore reconstruction supplants concentration (**C**) for absorption (μ_a) when solving the PMI minimization equation.

$$\Omega\left(\mu_a^{\lambda}\right) = \sum_{n=1}^{N} \left\| T_n^m(\lambda) - T_n^{\lambda}(\mu_a^{\lambda}) \right\|^2 \tag{2.8}$$

Through this change, processing time is greatly decreased and an unnecessary step is removed from the reconstruction process. A comparison of the two reconstruction processes is presented below in the form of a flowchart.

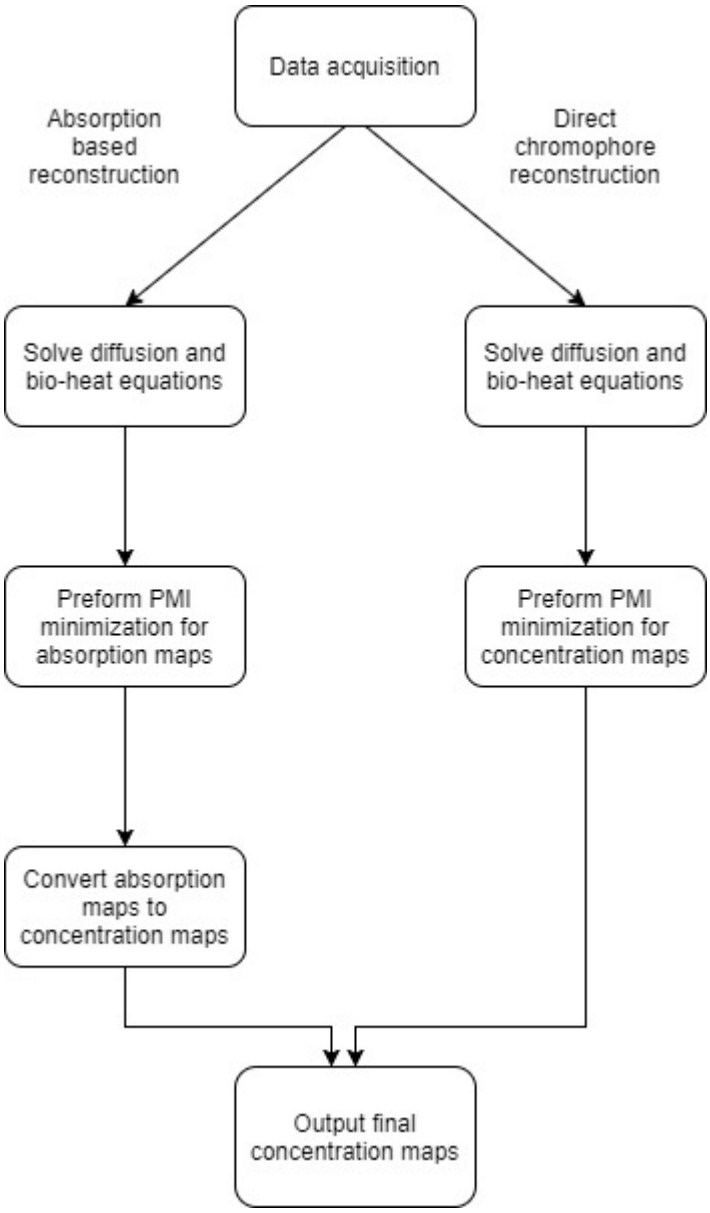

Figure 2.11 Comparison of two possible reconstruction methods

Clearly, as PMI moves forward it will be less computationally intensive to use direct chromophore reconstruction. With the system prototype complete validation with an optical phantom is necessary demonstrate its ability and validate its design.

Chapter 3

EXPERIMENTAL STUDIES

3.1 Experimental Goals

While our previous PMI system used illumination sources of a single wavelength, recent modifications have made possible the use of three sources of varying wavelengths. These additional illumination sources make possible the simultaneous reconstruction of multiple contrast agents. Specifically, we will be focusing on the system's ability to quantify simulated oxygenated and deoxygenated hemoglobin. We hope that such reconstruction will dramatically aid in the study of breast and oral cancer as it would enable noninvasive tumor characterization. We look forward to applying this technique to more accurately monitor gold nanoparticle distribution in-vivo as well as forming concentration gradients of various other exogenous agents.

Here, our system is tested with a cylindrical tissue mimicking agar phantom. The optical and thermal properties of the phantom were tuned to match simulation. Two 4mm inclusions were added to this phantom, each having 4% higher absorption than background media due to addition of optical dyes with certain absorption spectrums (QCR869A and QCR782E respectively). The goal of this experiment is to demonstrate that multi-wavelength PMI to accurately quantify the influence of QCR869A and QCR782E. A map of the phantom's absorption produced from experimental data will be compared to simulation. Similarly,

numerical estimates of the inclusions absorption values will be compared to simulation values. In doing so **aim 2** will be satisfied and the prototype will be considered validated.

3.2 Phantom Preparation

Careful phantom design is necessary to ensure accurate validation of the multi wavelength PMI prototype. These phantoms would need to demonstrate the system's ability to quantify the concentration of embedded contrasts agents and produce an accurate thermal map of the phantom as a whole. At our disposal were two specialized dyes; QCR869A and QCR782E.

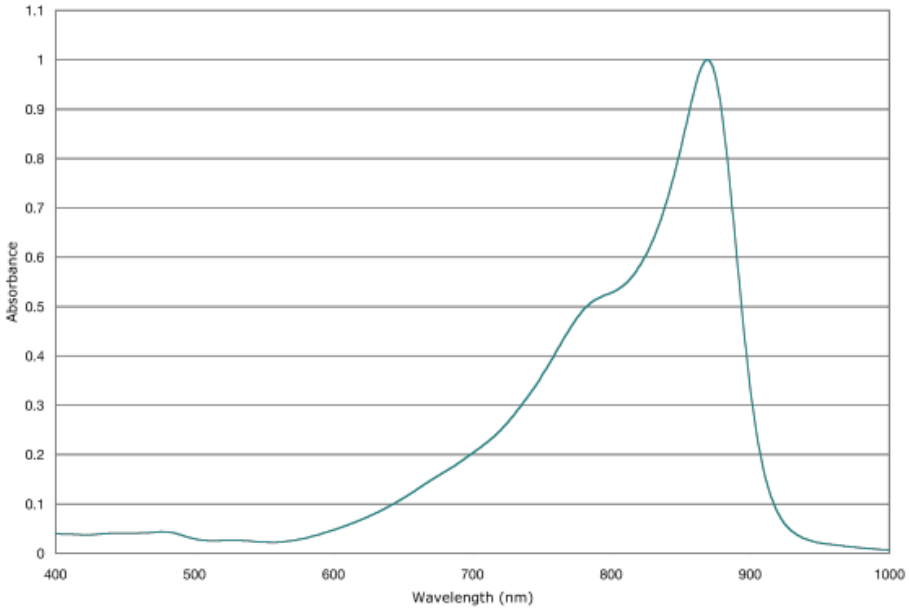

Figure 3.1 Absorption Spectrum of QCR869A [32]

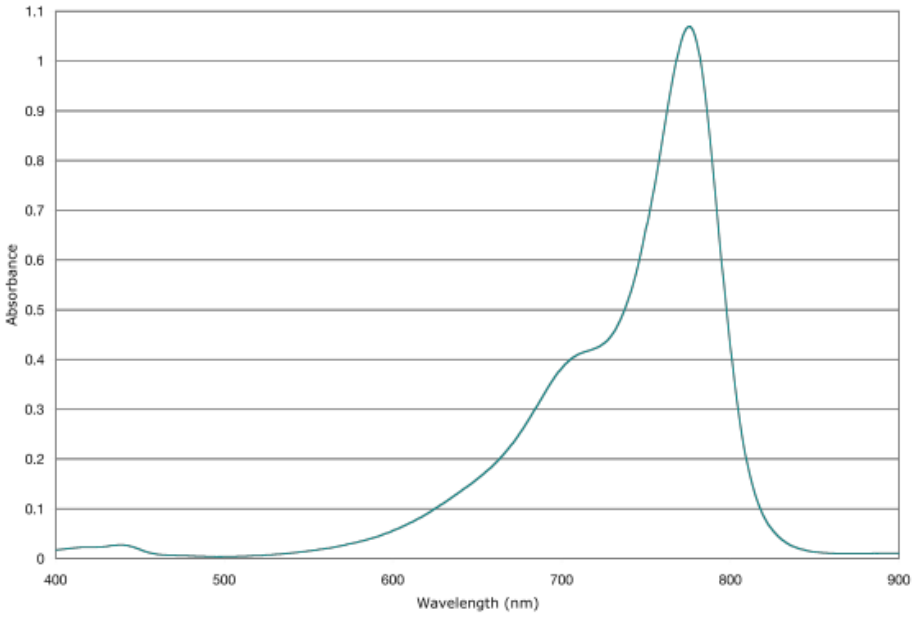

Figure 3.2 Absorption Spectrum of QCR782E [32]

These dyes were selected because their absorbance peaks closely match our lasers and their isosbestic point (around 800nm) is within the bulk of our measurement. Their isosbestic point also is fairly similar to that of oxy- and deoxy- hemoglobin. Spectrometer data calibrated the absorbance of the dyes for reconstruction purposes. This spectrometer data was collected by producing cuvettes of various combinations of contrast agents included in the final phantom.

Table 3.1 Real Absorption Values (mm^{-1})

	λ = 785nm	λ = 808nm	λ = 850nm
Left Inclusion (QCR869A)	**.0176**	**.0176**	**.0280**
Right Inclusion (QCR782E)	**.0195**	**.0134**	**.0096**
Background	**.0096**	**.0096**	**.0096**

The phantoms were agarose, with intralipid to mimic the scattering properties of living tissue and India ink to produce background absorption according to a formula used by my lab for many years. This formula was designed to have a μ_s similar of that to normal tissue [33]. A small amount of gadolinium was also added to the agar solution to enhance contrast in anatomical images by shortening the T1 and T2 relaxation rate.

The phantom was formed first as a 25mm cylinder with two 5mm cylindrical holes passing through axially 5mm below the surface. After it had set the holes were filled with an agarose solution containing QCR869A and QCR782E respectively. These dyes were added at a known concentration used to produce the control simulation visible in section 3.4.

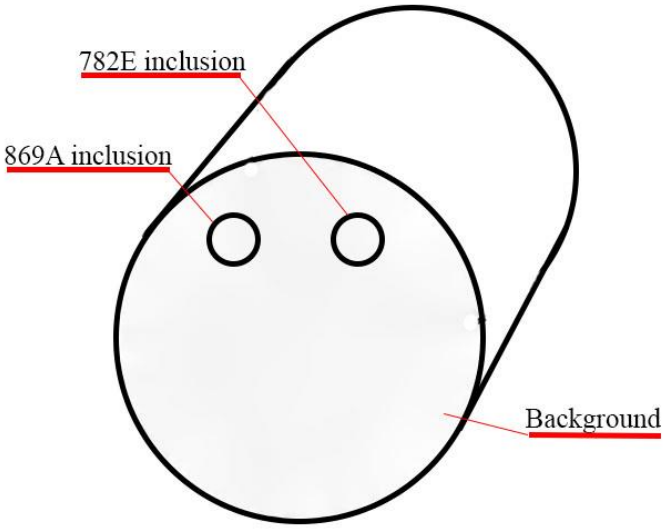

Figure 3.3 Diagram of agarose phantom with labeled inclusions

3.3 Data Acquisition

The MRT measurements are performed inside a Philips 3 Tesla Achieva system. PRF images are acquired using a gradient echo sequence using 60 and 12 ms as repetition and ET, respectively. The phantom is illuminated by each of the three laser diodes described in section 2.3. The laser diodes and their drivers are all positioned at the control room, at a safe distance from the MRI bore. Light is transported to the PMI interface located inside the MR bore using four 15 meter long optical fibers. The PMI interface consists of a specially designed RF coil with four windows for illumination and four ports that hold the collimation optics. The optical fibers

are connected to these ports such that, their output light is collimated by a 35-mm Newport optics aspherical lenses prior to reaching the sample positioned at the center of the RF coil. The laser power per unit area is set to the ANSI limits, confirmed by a power meter (PM100D, Thorlabs) [33].

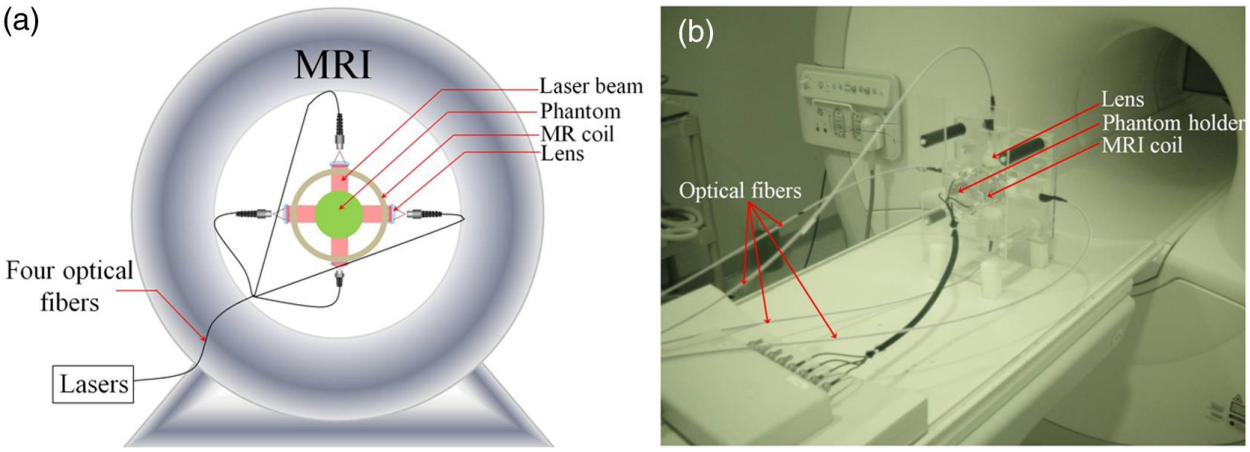

Figure 3.4 a. a schematic of PMI setup showing arrangement of instrumentation inside the MRI bore **b.** A photo of the PMI interface (a specially designed RF coil with four illumination windows and necessary collimation optics) on the MRI bed [34]

The MR temperature maps acquisition is synchronized with the laser drivers. Figure 3.5a shows the timeline of data acquisition. First, a T1 weighted low-resolution MR pilot image is acquired to localize the axial position of the laser probe. Once the axial plane located, a dynamic imaging set consisting of multiple frames (6 s each) is initiated. A gradient echo sequence is used to obtain a high-resolution phase image at each time point. The first baseline frame ($\varphi 0$) is acquired before turning-on the laser. After the laser is turned on, the phantom is illuminated from the top. During this heating phase, another frame is acquired (φ_i). Thus, the total PMI data

acquisition time is nearly 12 seconds per laser. After subtracting the baseline image (φ_0) from the image acquired during heating phase (φ_i), relative phase change for each pixel can be obtained and hence, a high-resolution image describing the temperature increase can be produced. Each pixel of this image serves as a measurement point to monitor the temperature increase. This temperature map is utilized as the final measurement map in reconstruction during the PMI minimization. Actually, more than one frame can also be acquired during the heating phase to increase SNR. Although, a perfect PMI reconstruction should be obtained using phase image acquired at the end of the heating cycle, a combination of several frames is often utilized [35]. Note that PMI data can be acquired continuously as long as the laser illumination is kept under ANSI limits [33] This process is repeated for each of the three light sources to produce three separate thermal maps.

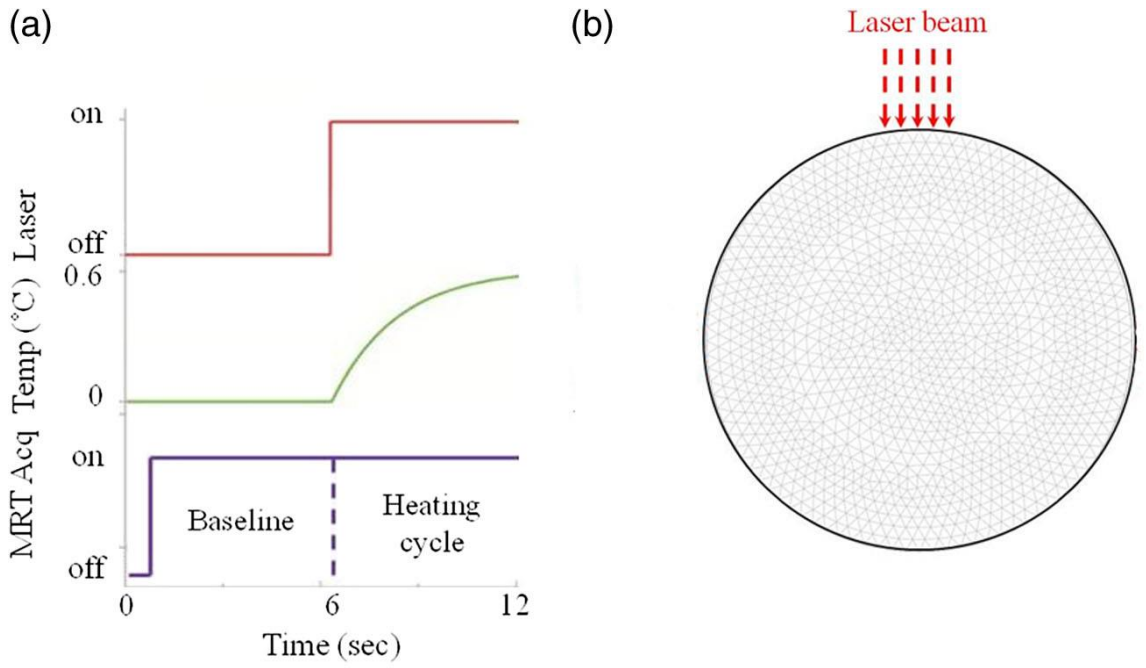

Figure 3.5 a. Timeline of PMI data acquisition comparing laser status, sample temperature, and MRT acquisition b. a simple diagram showing cross section of the phantom and the collimated laser illumination beam [33]

3.4 Results

After acquisition, we produce FEM simulation data to compare to our experimentally collected data. Pictured below are both simulation and experimental results. The mismatch between these two will determine the accuracy of our system to predicted outcomes.

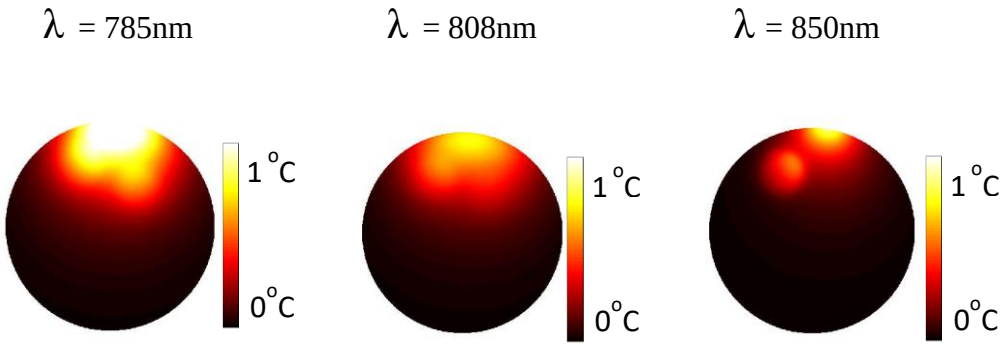

Figure 3.6 MRT Simulation Data

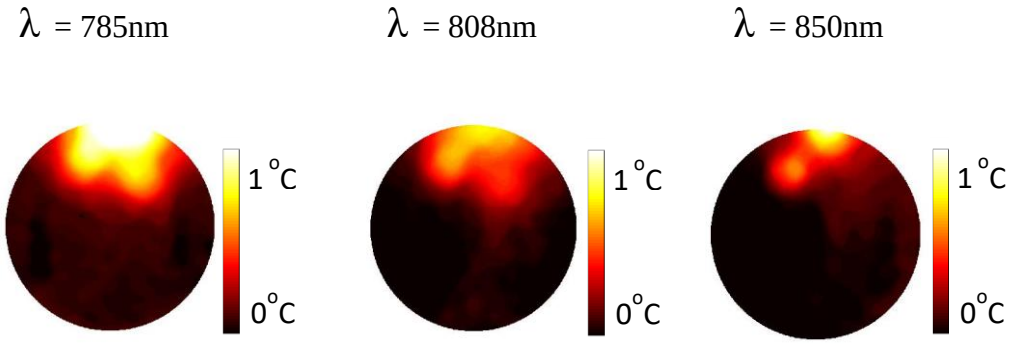

Figure 3.7 MRT Experimental Results

The above figures (3.6 and 3.7) portray the similarity between simulation and collected results. This very close relationship and very small mismatch visually implies the validity of our methods and the accuracy of our data relative to predictive modeling. From the experimental data absorption maps are reconstructed using the process described in Section 2.3 mathematical

modeling. Next an absorption reconstruction is preformed calibrated by tuning curves for the two QCR dyes collected earlier.

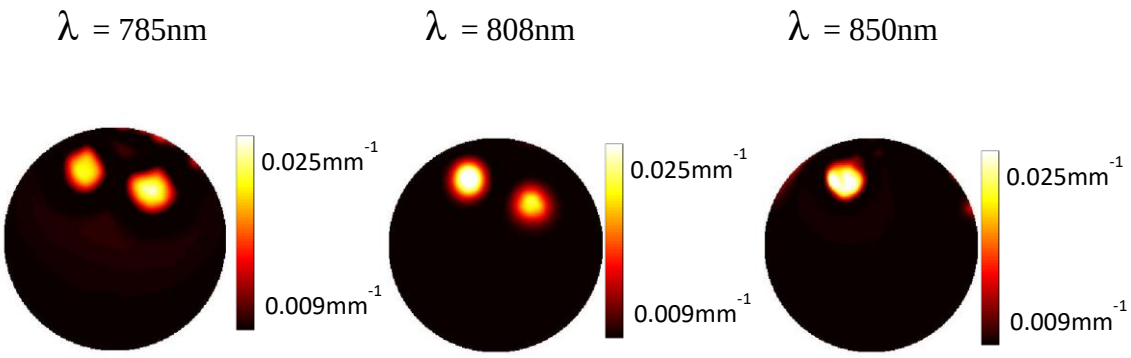

Figure 3.8 Reconstruction Results μa (mm^{-1})

The reconstructed absorption map intuitively matches prediction as the QCR782 inclusion is brighter in images captured with the lower wavelength sources, while the QCR869 inclusion is clearly favored in the images captured under high wavelength illumination. Data enabling a final comparison of numerical values between simulation and experimental reconstruction follow.

Table 3.2 Experimental Mean Absorption Values Calculated Over 4mm^2 Area With Standard Deviation and Error (mm^{-1})

	λ = 785nm	λ = 808nm	λ = 850nm
Left Inclusion (QCR869A)	**.0170±.0036 ε = 3.4%**	**.0154±.0026 ε = 12.5%**	**.0288±.0066 ε = 2.8%**
Right Inclusion (QCR782E)	**.0186±.0037 ε = 4.6%**	**.0134±.0015 ε = 0.0%**	**.0093±.0001 ε = 3.1%**
Background	**.0093±.0001 ε = 3.1%**	**.0093±.0001 ε = 3.1%**	**.0093±.0001 ε = 3.1%**

This table clearly demonstrates the accuracy of the data obtained by our multi-wavelength system's reconstructed data. The very small mismatch between expected and measured value validates our design and method. Further discussion of these results follows including a summary of the device and experiment and detailed discussion of the future prospects of this multi-wavelength PMI system.

In this thesis, a single wavelength PMI prototype was expanded to use multiple illumination sources of differing wavelengths. This modification aimed to enable e the system to quantify up to three tissue chromophores. Of specific interest was water, oxy-, and deoxy-

hemoglobin. Future researchers could also use the system to track exogenous contrast agents. The system is then carefully validated through phantom experimentation.

Our results presented in figure 3.8 demonstrate our system's ability to resolve, at MRI resolution, the phantom inclusions. The left inclusion, will be further referred to as Inc 1 (dye 1: QCR#869A): Ø 4 mm, C=0.014 M; the right being, Inc 2 (dye 2: QCR#782E): Ø 4 mm, C=0.009 M. The first column shows that at 785nm our system can detect both patches but can discriminate the absorbance after reconstruction. Table 3.1 and 3.2 demonstrate the accuracy of our reconstruction relative to real values. The second column demonstrates that at 808nm the QCR869A inclusion in visible since its absorption is higher in that wavelength and the other is not visible since it has very little absorption at 808nm. The third column depicts our system's ability to discriminate Inc 1 and completely reject Inc 2 at 850 nm both before and after reconstruction. Looking at figure 3.7 we can easily see that the right inclusion is matched to background at 850 nm. Some variance between image intensity is visible resulting from differences in laser power causing inhomogeneity in edge heating in the final thermal maps.

Chapter 4

DICUSSION AND CONCLUSIONS

4.1 Discussion

Optical imaging techniques, while varied and highly promising, are plagued by a lack of resolution and depth penetration. PMI offers the potential to overcome the possibility for clinician error in histological assessment. Histology requires a skilled physician to accurately diagnose and stage disease visually. Such visual diagnosis can produce erroneous diagnosis as a result of user error. In a time where many lab technicians and clinicians are overworked and under slept, the reduction of human judgment always brings a welcome reduction in false positive/negative diagnosis.

Although unlikely to dislodge biopsy and histology from is unanimous dominance of cancer diagnostics, PMI offers clinicians an alternative. PMI reduces patient discomfort and required technician skill when compared to conventional histology. The cost difference is offset by the fact that complex biopsies often involve MRI already. In essence PMI shares its aim for lowering the invasiveness of biopsy than many other optical techniques possess. This lower invasiveness makes optical imaging of high interest among researchers and clinicians alike.

In addition to depth of invasion, functional imaging modalities provide quantified tissue composition data. By using multiple wavelengths PMI can provide the very same functional/molecular information as other diffuse optical imaging techniques but with higher resolution and better quantitative accuracy. This ability could be used to track and quantify various chromophores. These could be either endogenous (as in oxy- or deoxy- hemoglobin) or

exogenous (in the form of injected contrast agents or nanoparticles). Both of which pose distinct advantages.

Our PMI experimental results support the superior performance of the PMI compared to other conventional diffuse optical imaging modalities. The accuracy with which we are able to resolve the position of the inclusion in reconstruction is clear from Figure 3.8. Such anatomical accuracy is a staple of MRI and the chief benefit of our system over conventional optical systems. Our system successfully estimated the dye concentration present in each sample with an error as low as 3%. Real data (Table 3.1) closely resembles MRT Results (Table 3.2), again lending to our systems stability and accuracy as well as the accuracy of our simulation methods.

Some slight artifacts in reconstruction may be a result of small cavitations in the phantom resulting from backfilling the inclusions or from uneven accumulation of chromophores. Also, our analytical method models the laser as a point source when it is actually a collimated beam with a diameter of ~13.5mm. This discrepancy in source size could yield slight artifacts particularly near the illuminated surface. Fortunately, these slight artifacts do not interfere with the quantitative accuracy of our method.

PMI has the ability to be used in applications with deeper probing depth with the addition of more laser sources to illuminate a subject from all sides. In essence, the systems main limitation is how deep light can penetrate while maintaining ANSI limits. Possibly the power could be slightly increased and more sources could be modified to make the system ready for preclinical studies.

4.2 Future Work

By modifying our previous PMI prototype to use three different wavelengths of NIR light, our system has become capable of discriminating between dyes of different absorption spectrum. It was able to approximate the absorption of these dyes with error as low as 3%. The updated model is a great step toward the ability to approximate the concentration of oxygenated and deoxygenated hemoglobin, or other contrast agents in vivo. Our PMI reconstruction algorithm successfully mapped the absorbers to anatomical images with complete accuracy at a standard voxel size of $1.2mm^3$. While this is a great result, it only validates our prototype. Future studies are needed to demonstrate in more accurate models the ability of the system to resolve the optical properties of diseased tissue such as cancerous lesions, at MRI resolution.

For future study, it would be ideal to dyes that more closely mirror the optical properties of oxy- and deoxy-hemoglobin or for an even more powerful study, use an animal tumor model. However, it appears the dyes used thus far, demonstrate the ability of the prototype. Our future research is geared toward readying the system for an *in-vivo* study possibly using a rat or hamster cancer model. Specifically, this system has great ability to aid in the study of oral cancer.

With the appropriate IRB approval, the design of an experiment using breast cancer patients would hold great possibility for advancing our understanding of tumor composition and prove beyond a shadow of a reasonable doubt that PMI is capable of being used for clinical research. The successful detection of tumor deeply embedded in breast tissue would constitute a substantial breakthrough. Currently very few imaging modalities have even attempted to quantify tumor composition, and those that have do so at a very low depth. PMI has a great potential for

imaging completely though a breast without major compression. This would require the use of four sources for each illumination wavelength. This will be a simple modification given the already completed design of a circuit board to house the necessary laser drivers.

Ultimately, a highly impactful application of PMI would be to track gold nanoparticles. As described in Section 1.3, cutting edge research has demonstrated the ability of anti-EGFR conjugated gold nanoparticles to target oral cancer. Also, as discussed in Section 1.3 PMI offers a superior ability to track such nanoparticles than any currently used methods. These two technologies used in conjunction would constitute a possible breakthrough. Such a combination could bring breakthrough understanding of cancer, its lifecycle, and advance its treatment. Ultimately with proper research supporting its clinical transition, PMI could have a great impact on oncology.

References

[1] Johnson, Newell Walter, et al. "Global oral health inequalities in incidence and outcomes for oral cancer causes and solutions
[2] Ryerson, A. Blythe, et al. "Burden of potentially human papillomavirus-associated cancers of the oropharynx and oral cavity in the US, 1998–2003."Cancer 113.S10 (2008): 2901-2909.
[3] [De Veld, D. C. G., et al. "The status of in vivo autofluorescence spectroscopy and imaging for oral oncology." Oral oncology 41.2 (2005): 117-131]
[4] “Category:Oral Cancer.” *Category:Oral Cancer - Wikimedia Commons*, Creative Commons, 2017, commons.wikimedia.org/wiki/Category:Oral_cancer.
[5] Bock, O. (2017). *A history of the development of histology up to the end of the nineteenth century*. [online] Research-journal.net. Available at: https://www.research-journal.net/en/A-history-of-the-development-of-histology-up-to-the-end-of-the-nineteenth-century.html [Accessed 26 Aug. 2017].
[6] “Category:Histopathology.” *Category:Histopathology - Wikimedia Commons*, Creative Commons, 2017, commons.wikimedia.org/wiki/Category:Histopathology#/media/File:Breast_carcinoma_in_a_lymph_node.jpg.
[7] Konecky, Soren D., et al. "Quantitative optical tomography of sub-surface heterogeneities using spatially modulated structured light." *Optics express*17.17 (2009): 14780-14790.
[8] Malini, R., et al. "Discrimination of normal, inflammatory, premalignant, and malignant oral tissue: a Raman spectroscopy study." Biopolymers 81.3 (2006): 179-193.
[9] [PWS] Kim, Chang Soo, et al. "Enhanced detection of early-stage oral cancer in vivo by optical coherence tomography using multimodal delivery of gold nanoparticles." *Journal of biomedical optics* 14.3 (2009): 034008-034008.
[10] [CMP] Wilder-Smith, Petra, et al. "Noninvasive imaging of oral premalignancy and malignancy." *Journal of biomedical optics* 10.5 (2005): 051601-051601.
[11] Tromberg, Bruce J., et al. "Assessing the future of diffuse optical imaging technologies for breast cancer management." *Medical physics* 35.6 (2008): 2443-2451.
[12] Optical properties of biological tissues: a review - Oregon Medical ...." 10 May. 2013, http://omlc.org/news/dec14/Jacques_PMB2013/Jacques_PMB2013.pdf. Accessed 21 Feb. 2017.
[13] Lin, Yuting, et al. "Photo-magnetic imaging: optical imaging at MRI resolution."Biomedical Optics. Optical Society of America, 2012.
[14] [Nouizi, Farouk, et al. "Real-time photo-magnetic imaging." *Biomedical optics express* 7.10 (2016): 3899-3904.
[15] El-Sayed, Ivan H., Xiaohua Huang, and Mostafa A. El-Sayed. "Surface plasmon resonance scattering and absorption of anti-EGFR antibody conjugated gold nanoparticles in cancer diagnostics: applications in oral cancer." *Nano letters* 5.5 (2005): 829-834.”
[16] Tromberg, Bruce. “What Is DOSI.” *DOSI*, Beckman Laser Institute, 2017, dosi.bli.uci.edu/research/.

[17] "WSLB-830-012-H." *Photonics, Optical & Fiber Optic Products - Specpick.com*, 2017, www.gophotonics.com/products/laser-diodes/wavespectrum-laser-inc-/30-212-wslb-830-012-h.
[18] "2W, 3W, 808nm, Fiber Coupled Single Emitter Diode Laser(CW)." *Global Sources*, 2017, www.globalsources.com/si/AS/globaltyson/6008837510927/pdtl/2W/1093979278.htm.
[19] "LDX-3640-860-FC: 860nm Fiber Coupled Laser Diode." *Solid State Lasers and Laser Diodes from RPMC Lasers Inc*, 2017, www.rpmclasers.com/product/ldx-3640-860-fc/.
[20] "PLD5000 5 A Laser Diode Driver, PCB Mount." *PLD5000 5 A Laser Diode Driver*, Wavelength Electronics, 2017, www.teamwavelength.com/products/product.php?part=34&view=specs#tabs.
[21] "Heat Sink Calculator." *All About Circuits*, EETech Media, 2017, www.allaboutcircuits.com/tools/heat-sink-calculator.
[22] "4.600' Wide Extruded Aluminum Heatsink." *HeatsinkUSA*, HeatsinkUSA, 2017, www.heatsinkusa.com/4-600-wide-extruded-aluminum-heatsink/.
[23] Nouizi, F., et al. "An accelerated photo-magnetic imaging reconstruction algorithm based on an analytical forward solution and a fast Jacobian assembly method." *Physics in medicine and biology* 61.20 (2016): 7448.
[24] Nouizi, F. "Preclinical, fluorescence and diffuse optical tomography: non-contact instrumentation, modeling and time-resolved 3D reconstruction." (2011).
[25] S. Arridge, Photon-measurement density functions. Part I: Analytical forms, Appl. Opt. 34 (1999) 7395-7409.
[26] M. Schweiger, S.R. Arridge, M. Hiraoka, D.T. Delpy, The finite element method for the propagation of light in scattering media: boundary and source conditions, Med Phys 22(11 Pt 1) (1995) 1779-92.
[27] J. Hebden, S. Arridge, D. Delpy, Optical imaging in medicine. I. Experimental techniques, Phys Med Biol 42 (1997) 825 - 840.
[28] S.H. Diaz, G. Aguilar, E.J. Lavernia, B.J.F. Wong, Modeling the thermal response of porcine cartilage to laser irradiation, IEEE, Selected Topics in Quantum Electronics, 2001, pp. 944 - 951.
[29] Y. Lin, H. Gao, D. Thayer, A.L. Luk, G. Gulsen, Photo-magnetic imaging: resolving optical contrast at MRI resolution, Phys Med Biol 58(11) (2013) 3551-62.
[30] E.H. Wissler, Pennes' 1948 paper revisited, J Appl Physiol (1985) 85(1) (1998) 35-41.
[31] F. Nouizi, A. Luk, D. Thayer, Y. Lin, S. Ha, G. Gulsen, Experimental validation of a high-resolution diffuse optical imaging modality: photomagnetic imaging, J Biomed Opt 21(1) (2016) 16009.
[32] "NIR Dyes." *NIR Dyes for Solvent Systems | QCR Solutions Corp*, QCR Solutions Corp, 2017, www.qcrsolutions.com/Site/Near_Infrared_%28NIR%29_Dyes___QCR_Solutions_Corp.html.
[33] Kato, Hirokazu, et al. "Composition of MRI phantom equivalent to human tissues. "Medical physics32. 10 (2005): 3199-3208.
[34] Erkol, Hakan, et al. "An Analytical Approach for Temperature Distribution in Tissue." *Optical Tomography and Spectroscopy*. Optical Society of America, 2016.
[35] M. Schweiger et al., "The finite element method for the propagation of light in scattering media: boundary and source conditions," Med. Phys. 22, 1779–1792 (1995).http://dx.doi.org/10.1118/1.597634